

Cite this: *J. Mater. Chem. A*, 2020, **8**, 3845

Large area high-performance bismuth vanadate photoanode for efficient solar water splitting†

Meirong Huang,^a Wenhai Lei,^b Min Wang,^a Shuji Zhao,^c Changli Li,^d Moran Wang^b and Hongwei Zhu^{id}*^a

Commercial-scale photoelectrochemical (PEC) water splitting devices have been proved to be cost-competitive with fossil-based fuels. Nevertheless, large-scale PEC water splitting cells with high performance have not yet been demonstrated, and controllably scaling up high-performance photoelectrodes still remains challenging. Typically, bismuth vanadate (BiVO₄) has been regarded as one of the most efficient photoanodes for use in PEC water splitting because of its well-suited band structure. However, state-of-the-art PEC performances achieved with BiVO₄ photoanodes to date have generally been tested on small scales (<1 cm²), due to the nonuniformity of the scaled-up photoactive films, increased resistive losses and inhomogeneous potential distribution in scaled-up substrates, non-linear diffusion of reactants and resultants toward scaled-up photoanodes and so on. Here, a uniform scaled-up precursor (BiOI) film was prepared *via* a spatial-current-density-distribution-regulated electrodeposition method with a tilt-electrode-configuration. The as-prepared BiOI film was covered with a thin vanadium source layer and then converted to BiVO₄ film *via* a modified thermal-chemical conversion method. The photocurrent density for sulfite oxidation of the 54.32 cm² BiVO₄ photoanode (~2.55 mA cm⁻² at 1.23 V_{RHE}) was the highest value yet reported, and it was comparable with that of the 1.66 cm² BiVO₄ photoanode (~2.85 mA cm⁻² at 1.23 V_{RHE}). To reduce resistive losses and improve the homogeneity of distributed potential in the FTO substrate, metal grids were deposited on the BiVO₄ photoanode *via* thermal evaporation. The maximum fill factor of the photocurrent density curve of the scaled-up BiVO₄ photoanode was raised from ~29 to ~44.5%. After the uniform coating of an oxygen evolution catalyst (OEC) layer that was formed by connecting tannin acid molecules with metal ions, the photoanode achieved a photocurrent density of ~2.23 mA cm⁻² at 1.23 V_{RHE} and ~0.83% STH conversion efficiency at 0.65 V_{RHE}. Finally, the stability test was conducted in a designed test system with water circulation to facilitate diffusion of generated oxygen. The scaled-up OEC/BiVO₄ photoanode showed <4% decay after operating under harsh conditions for 5 h.

Received 15th December 2019
Accepted 20th January 2020

DOI: 10.1039/c9ta13715g

rsc.li/materials-a

1. Introduction

Direct conversion of solar energy to hydrogen and oxygen by water splitting is an increasingly attractive way to both energy production and storage. Several approaches have been employed to realize solar water splitting, including photocatalysis and photoelectrolysis. Photoelectrolysis can be accomplished by using photoelectrochemical (PEC) cells or

photovoltaic (PV) cells connected to electrochemical (EC) cells.^{1,2} The technical and economic feasibility analysis of large-scale photochemical and photoelectrochemical water splitting has been conducted, and commercial-scale solar water splitting devices have been proved to be cost-competitive with fossil-based fuels.^{3,4} If a catalytic material is made to meet the performance target with an appropriate plant-scale technology, the production cost is consistent with the Department of Energy's target threshold cost of 2.00–4.00\$ per kg H₂,³ and the energy payback time is ~8 years under base-case conditions.⁴ However, only a few research studies about the scale-up of photocatalytic and photovoltaic-driven electrochemical (PV-EC) water splitting cells have been conducted. Panel-type reactors for large-scale photocatalytic water splitting have been fabricated, in which carbon nitride (CN) and SrTiO₃ photocatalyst are immobilized on stainless steel and frosted glass plates *via* drop-coating, respectively.^{5,6} Silicon solar cells connected to metal or metal oxide electrocatalysts, so called PV-EC cells, have

^aState Key Laboratory of New Ceramics and Fine Processing, School of Materials Science and Engineering, Tsinghua University, Beijing 100084, China. E-mail: hongweizhu@tsinghua.edu.cn

^bDepartment of Engineering Mechanics, Tsinghua University, Beijing 100084, China

^cState Key Laboratory of Tribology, School of Aerospace Engineering, Tsinghua University, Beijing 100084, China

^dDepartment of Chemistry, The University of British Columbia, 2036 Main Mall, Vancouver, BC V6T1Z1, Canada

† Electronic supplementary information (ESI) available: Materials and methods, supplementary figures. See DOI: 10.1039/c9ta13715g

been fabricated *via* laser processing.^{7,8} Nevertheless, the safety risk and separation process of cogenerated H₂ and O₂ will still lead to great uncertainty in the operation of photocatalytic water splitting. The high conversion efficiency of PV-PEC cells is restricted by both incident photon-to-current conversion efficiency of PV cells and electrocatalytic efficiency of EC cells, which is a key parameter driving costs for this system.³ Therefore, the “Holy Grail” of solar energy conversion and storage is PEC water splitting. However, large-scale PEC water splitting cells with high performance have not yet been demonstrated, and controllable scale-up of high-performance photoanodes and photocathodes is the challenge.

The bottleneck of water splitting is the water oxidation half reaction, which is a four-electron oxidation process of two water molecules. Bismuth vanadate (BiVO₄) has been regarded as one of the most efficient photoanodes for use in water oxidation, because it can absorb a significant portion of visible light with a bandgap of ~2.4 eV and has favorable band positions that are well-suited for driving the oxygen evolution reaction (OER). In addition, BiVO₄ is composed of earth-abundant elements and known to be non-toxic and stable against chemical corrosion in near-neutral solution. Therefore, PEC cells based on BiVO₄ photoanodes are promising for solar water splitting at large scales.^{9–11} In reality, it is worth noting that the state-of-the-art performances achieved with BiVO₄ photoanodes have generally been tested on small scales with photoactive areas typically less than 1 cm².^{12–15} Scaling up BiVO₄ photoanodes while retaining their high performances still remains challenging.¹¹ Experimental studies indicate that the photoactive area has a significant and negative effect on photocurrent density (*i.e.*, “areal effect”).^{9,10,16,17} The severe reduction in photocurrent density of scaled-up photoelectrodes is mainly attributed to the nonuniformity of scaled-up photoactive films, increased resistive losses of scaled-up substrates, non-linear diffusion of reactants and resultants toward scaled-up photoanodes and so on. In addition, theoretical studies indicate that the inhomogeneous in-plane potential distribution in a scaled-up electrode, along with bubble formation and accumulation on the surface of the electrode, is responsible for the severe reduction in the photocurrent density of a scaled-up photoelectrode, which in turn generates design requirements for electrode geometry and configuration in a PEC reactor.^{18–21}

Electrodeposition (ED) has been proved to be a cost-effective and efficient industrial process.²² Small-scale BiVO₄ photoanodes prepared *via* ED together with a thermal-chemical conversion (TCC) method have shown outstanding PEC performances for the OER.^{13,14,23,24} Herein, we present a simple, efficient and scalable preparation method based on the ED-TCC method to prepare uniform scaled-up BiVO₄ photoanodes with high performance. Metal grids were evaporated on BiVO₄ photoanodes to reduce resistive losses and improve the homogeneity of distributed potential in scaled-up FTO substrates, and thus increase PEC performances of scaled-up BiVO₄ photoanodes. Finally, oxygen evolution catalysts (OECs) were deposited on the surface of BiVO₄ photoanodes to accelerate water oxidation kinetics, and the stability test was conducted in

a designed test system with water circulation to facilitate diffusion of generated oxygen.

2. Results and discussion

2.1 Preparation of scaled-up BiOI and BiVO₄ films

Nanoporous BiVO₄ films were prepared *via* a modified ED-TCC method. BiOI films were firstly electrodeposited on FTO substrates in a three-electrode cell at static potentials. A series of control experiments were conducted by changing the deposition potential (ESI Fig. S1†). In addition, electrodeposition with different electrode configurations was investigated experimentally and computationally (ESI Fig. S2–S4†). Finite element analysis based on a bipole type electrode in three-dimension (3D) was performed to explore the homogeneity of spatial-current-density-distribution in FTO substrates under different electrode configurations. Results indicated that uniform scaled-up BiOI films could not be prepared at any deposition potential and any electrode spacing under a parallel-electrode-configuration, because of the inhomogeneous distribution of current density as a function of spatial coordinates in the FTO substrate at a fixed applied potential (Fig. 1a). However, scaled-up BiOI films prepared under a tilt-electrode-configuration showed that the inhomogeneity could be improved by choosing a right electrode angle θ of the FTO substrate, which could be varied from 14° to 32° and even larger. The increased electrode angle contributed to improving the homogeneity of distributed current density in the FTO substrate (Fig. 1b). The possible mechanism was discussed in the ESI.† As expected, photographs of as-prepared BiOI films showed that the sample

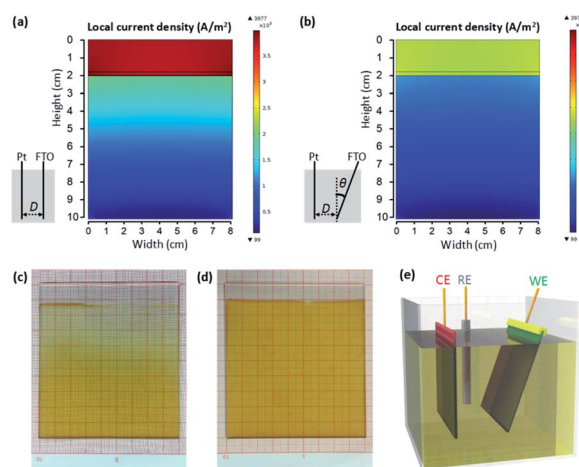


Fig. 1 Spatial-current-density-distribution in FTO electrodes under different electrode configurations (the insets show the corresponding schematic diagrams): (a) parallel-electrode-configuration ($D = 1$ cm, $\theta = 0^\circ$), (b) tilt-electrode-configuration ($D = 1$ cm, $\theta = 20^\circ$), modelled using COMSOL Multiphysics. Photographs of as-prepared BiOI films on FTO substrates *via* the SCDDR-ED method with different electrode configurations: (c) parallel-electrode-configuration ($D = 1$ cm, $\theta = 0^\circ$), (d) tilt-electrode-configuration ($D = 1$ cm, $\theta = 20^\circ$), the applied potential was -0.25 V_{Ag/AgCl}, and the deposition time was 300 s. (e) Schematic diagram of a tilt-electrode-configuration in a three-electrode reactor for electrodeposition.

prepared under a tilt-electrode-configuration exhibited better uniformity (Fig. 1c and d), corroborating well with computational results. In addition, scanning electron microscope (SEM) images showed good microscopic uniformity of the sample prepared under a tilt-electrode-configuration (ESI Fig. S5†).

In short, the spatial-current-density-distribution-regulated electrodeposition (SCDDR-ED) method realized by changing the electrode configuration was efficient for the preparation of uniform scaled-up BiOI films. The tilt-electrode-configuration of the SCDDR-ED method is shown schematically in Fig. 1e, consisting of $9 \times 10 \text{ cm}^2$ FTO as the working electrode (WE), a $9 \times 9 \text{ cm}^2$ Pt mesh as the counter electrode (CE) and a saturated Ag/AgCl electrode as the reference electrode (RE) separated by the electrolyte prepared according to previous reports (see details in the ESI†).^{15,24}

Since the PEC performance of the BiVO_4 photoanode was significantly related to the uniformity of BiVO_4 film, the BiOI film was uniformly coated with a thin vanadium source layer before annealing to realize the conversion of BiOI film to BiVO_4 film without affecting the uniformity. A schematic diagram of the modified thermal-chemical conversion (MTCC) method is shown in Fig. 2a. Thermal diffusion of the vanadium source, removal of excess vanadium source and rapid drying of the thin vanadium source layer could ensure uniform coating of a thin vanadium source layer on the BiOI film. Photographs and SEM images of the as-prepared BiOI film, BiOI film coated with a thin vanadium source layer and BiVO_4 film of size $9 \times 10 \text{ cm}^2$ indicated successful conversion with well-maintained uniformity

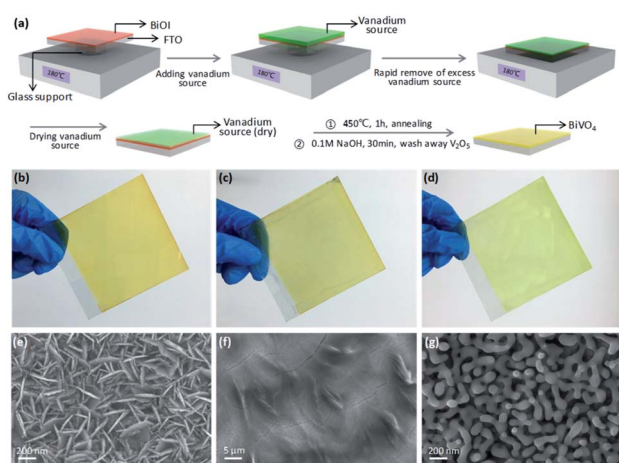


Fig. 2 (a) Schematic diagram of the MTCC method: BiOI film was placed on a glass support above a heating plate ($180 \text{ }^\circ\text{C}$); 1.5 mL vanadium source solution was added to the surface of BiOI film *via* drop-casting; after thermal diffusion of the vanadium source and evaporation of the solvent (7–8 min), the excess vanadium source was removed by a quick contact at the bottom edge of the film with a filter paper, and a very thin vanadium source layer was retained on the surface of BiOI film; the film was then placed on the heating plate ($180 \text{ }^\circ\text{C}$) directly to dry the thin vanadium source layer rapidly; the as-prepared film was transferred into a muffle furnace and converted to BiVO_4 film, and the as-annealed film was soaked in NaOH solution to wash away V_2O_5 (by-product) from the surface of BiVO_4 . Photographs and SEM images of (b and e) BiOI film, (c and f) BiOI film coated with a thin vanadium source layer and (d and f) BiVO_4 film ($9 \times 10 \text{ cm}^2$).

(Fig. 2b–g, see details in ESI Fig. S6 and S7†). BiOI nanosheets were converted to BiVO_4 nanostructures with a bandgap of $\sim 2.4 \text{ eV}$ (ESI Fig. S8†).

2.2 Sulfite oxidation of scaled-up BiVO_4 photoanodes

To investigate the “areal effect”, scaled-up BiVO_4 films were cut into several small pieces with different photoactive areas. PEC performances of BiVO_4 photoanodes with varying photoactive areas were studied by linear sweep voltammetry (LSV) and electrochemical impedance spectroscopy (EIS) in a three-electrode configuration, using 0.1 M potassium borate solution containing 0.5 M Na_2SO_3 ($\text{pH} = 9.3$), under AM 1.5G 1 sun back illumination (see details in the ESI†). Since sulfite oxidation was thermodynamically and kinetically favored compared to water oxidation,^{23,25} measuring the photocurrent density for sulfite oxidation enabled the investigation of the PEC performance of the BiVO_4 photoanode independent of its poor water oxidation kinetics. In addition, current density caused by backscattered light (J_B), together with dark current density (J_D) was estimated by completely blocking the back of the photoanode with a light proof tape and turning on a solar simulator. Part of light that bypassed the photoanode on its periphery got reflected or backscattered by the reactor to backlight the photoanode to generate J_B . The corrected photocurrent density $J_C = J - (J_B + J_D)$, where the uncorrected photocurrent density J was measured by directly illuminating the photoanode.²⁶

As shown in Fig. 3a (see details in ESI Fig. S9†), a maximum photocurrent density (up to $\sim 2.85 \text{ mA cm}^{-2}$ at an applied potential of $1.23 \text{ V}_{\text{RHE}}$) and a low onset potential ($\sim 0.2 \text{ V}_{\text{RHE}}$) were observed for the 1.66 cm^2 BiVO_4 photoanode. The photocurrent density of BiVO_4 photoanodes reduced slightly with the

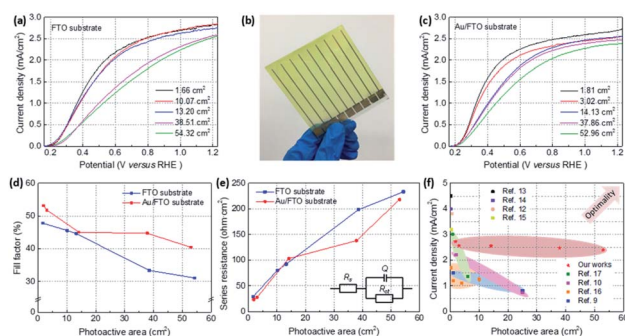


Fig. 3 PEC performances (sulfite oxidation) of BiVO_4 photoanodes. (a) LSV scans for the J_C of BiVO_4 photoanodes with different photoactive areas (FTO substrate). (b) Photograph of the BiVO_4 film deposited on an Au/FTO substrate. (c) LSV scans for the J_C of BiVO_4 photoanodes with different photoactive areas (Au/FTO substrate). (d) The maximum fill factor (FF) derived from J_C is depicted as a function of photoactive area for BiVO_4 photoanodes deposited on different substrates. (e) Series resistance (R_s) is depicted as a function of photoactive area for BiVO_4 photoanodes deposited on different substrates (the inset shows the equivalent circuit diagram). (f) Summary of some high-performance pure BiVO_4 photoanodes without doping and some scaled-up BiVO_4 photoanodes from references (the same color labeled and covered data were obtained from the same work), and our work. These photocurrent densities were recorded at $1.23 \text{ V}_{\text{RHE}}$.

increase of photoactive area. The losses reflected mainly on a decrease in fill factor (FF) with a minor loss in the photocurrent density at $1.23 V_{\text{RHE}}$. Here, the fill factor of the BiVO_4 photoanode is defined as the relationship of the local current J , local potential V , onset potential (V_{onset} , $\sim 0.2 V_{\text{RHE}}$) and photocurrent density at $1.23 V_{\text{RHE}}$ ($J_{1.23}$) similar to the fill factor of solar cells, namely $\text{FF} = \frac{J(1.23 - V)}{J_{1.23}(1.23 - V_{\text{onset}})}$. The photocurrent density at $1.23 V_{\text{RHE}}$ of the 54.32 cm^2 BiVO_4 photoanode ($\sim 2.55 \text{ mA cm}^{-2}$) was comparable with that of the 1.66 cm^2 BiVO_4 photoanode. The slight decrease confirmed the excellent uniformity of BiVO_4 photoanodes, indicating the excellent scalability and reproducibility of the preparation method. The decrease in photocurrent density of scaled-up BiVO_4 photoanodes could be attributed to increased resistive losses of scaled-up FTO substrates that were confirmed by EIS curves, inhomogeneously distributed potential in scaled-up FTO substrates and the non-linear diffusion of reactants and resultants toward scaled-up photoanodes, leading to restriction of charge separation and charge transfer in photoanodes.^{9,10,16,18} Predicted by the original Gärtner–Butler equation, the resulting serious charge carrier recombination could considerably decrease the photocurrent density thus the fill factor of photoanodes.¹⁸ Therefore, the degradation in performance caused by these factors required careful design of electrode geometry and configuration in a PEC reactor in turn, to further improve the PEC performances of scaled-up photoelectrodes.

To reduce resistive losses and improve the homogeneity of distributed potential in FTO substrates, Au metal fingers (finger-like metal grids) were deposited on FTO substrates *via* thermal evaporation through a mask. Similarly, uniform scaled-up BiOI films could also be deposited on Au metal fingers/FTO (Au/FTO) substrates *via* the SCDDR-ED method with a tilt-electrode-configuration, and the required deposition potential reduced significantly because of the superior conductivity of Au/FTO substrates (ESI Fig. S1 and S6†). After uniform coating of the vanadium source layer and subsequent annealing *via* the MTCC method, one of the as-prepared uniform scaled-up BiVO_4 films is shown in Fig. 3b and S6b (ESI†). Scaled-up BiVO_4 films were also cut into several small pieces to investigate the “areal effect”; similarly, J_{B} and J_{D} were measured to correct the recorded photocurrent density J . According to Fig. 3c (see details in the ESI Fig. S10†), a maximum photocurrent density ($\sim 2.72 \text{ mA cm}^{-2}$ at $1.23 V_{\text{RHE}}$) and a low onset potential ($\sim 0.2 V_{\text{RHE}}$) were recorded for the 1.81 cm^2 BiVO_4 photoanode deposited on the Au/FTO substrate. They were slightly different from those of the 1.66 cm^2 BiVO_4 photoanode deposited on the FTO substrate, which could be attributed to different preparation conditions. The photocurrent density of BiVO_4 photoanodes deposited on Au/FTO substrates followed a decreasing trend with respect to photoactive area, similar to those deposited on FTO substrates. However, the higher fill factor and decreased resistive losses of BiVO_4 photoanodes deposited on Au/FTO substrates also indicated the superior conductivity of Au/FTO substrates, which could increase the actual applied potential and improve the homogeneity of distributed potential in scaled-up substrates.

To draw an accurate comparison between the performances of BiVO_4 photoanodes deposited on different substrates, the maximum FF calculated from the corrected photocurrent density using $\text{FF} = \frac{J(1.23 - V)}{J_{1.23}(1.23 - V_{\text{onset}})}$ is depicted as a function of photoactive area in Fig. 3d. In addition, EIS curves were fitted according to the equivalent circuit diagram shown in the inset of Fig. 3e, where the resulting R_{s} and R_{ct} represent series resistance and charge carrier transport resistance, respectively. Series resistance is also depicted as a function of photoactive area in Fig. 3e. Clearly, the maximum FF of BiVO_4 photoanodes with different photoactive areas were significantly improved by Au metal fingers due to the superior conductivity, except for the 14.13 cm^2 BiVO_4 photoanode deposited on the Au/FTO substrate whose FF was also affected by the strip shape of the electrode (ESI Fig. S11†). Higher resistive losses of the strip-shaped photoanode were confirmed by its larger series resistance, compared with the photoanode deposited on the FTO substrate with a comparable area. Therefore, resistive losses of scaled-up photoelectrodes especially the amplification from the far-end of the electrode were non-ignorable.

Fig. 3f shows a summary of some high-performance pure BiVO_4 photoanodes without doping (their photoactive areas were typically less than 1 cm^2) and some scaled-up BiVO_4 photoanodes from references, and our studies, which were tested in the presence of an OEC or a hole scavenger. Observed from Fig. 3c, BiVO_4 photoanodes deposited on Au/FTO substrates achieved a photocurrent density at $1.23 V_{\text{RHE}}$ of 2.72, 2.56, 2.55, 2.47, and 2.39 mA m^{-2} with a photoactive area of 1.81, 3.02, 14.13, 37.86, and 52.96 cm^2 , respectively. Most of them were the highest values yet reported among all BiVO_4 photoanodes, indicating that the simple, efficient and scalable preparation method was promising to prepare large-scale high-performance BiVO_4 photoanodes for practical solar water splitting.

Furthermore, a new, simple, effective yet economical approach was proposed to prepare non-noble metal grids on photoanodes (ESI Fig. S12†). Learning from the metal contact structure of solar cells, rib-like Ag metal grids were patterned on the BiVO_4 photoanode (ESI Fig. S13†) to further reduce resistive losses and improve the homogeneity of distributed potential in the scaled-up substrate. As expected, the maximum fill factor of the photocurrent density curve of the scaled-up BiVO_4 photoanode was further increased to $\sim 44.5\%$.

2.3 Water splitting of scaled-up OEC/ BiVO_4 photoanodes

Since the water oxidation performance of the BiVO_4 photoanode was restricted by poor water oxidation kinetics, introduction of an OEC layer could facilitate the water oxidation reaction by lowering the activation energy of the OER reaction and passivating surface charge recombination sites on the surface of BiVO_4 . Much effort has been made in preparing highly active OECs for BiVO_4 -based photoanodes, and Ni/Fe/Co-based OECs were found to be more efficient for the OER (ESI Fig. S14†). To find out an appropriate method for preparing scaled-up OEC/ BiVO_4 photoanodes, an NiFe-based OEC was prepared by four different methods (ESI Fig. S15–S17†). Comparison of their PEC

performances suggested that the Dip-TA method, where BiVO_4 was dipped in a solution containing tannic acid (TA) and $\text{Ni}^{2+}/\text{Fe}^{3+}$ ions, was a simple, low-cost and scalable method for preparing highly active and stable $\text{OEC}_{\text{Dip-TA}}/\text{BiVO}_4$ photoanodes, and the super hydrophilicity of TA was of benefit to inhibit bubble accumulation on the surface of BiVO_4 photoanodes, especially for scaled-up photoanodes (ESI Fig. S18 and S19†).

The SEM image presented an identical surface morphology of $\text{OEC}_{\text{Dip-TA}}/\text{BiVO}_4$ film (Fig. 4a), where the OEC layer formed 2D networks by connecting TA molecules with metal ions. The PEC performance of the $\text{OEC}_{\text{Dip-TA}}/\text{BiVO}_4$ photoanode was studied in a three-electrode configuration, using 0.1 M potassium borate solution (pH = 9.35), under AM 1.5G 1 sun back illumination. The photocurrent density was corrected with J_B and J_D . After the deposition of the OEC layer, the onset potential of the BiVO_4 photoanode at small scale was shifted from ~ 0.42 to $\sim 0.25 V_{\text{RHE}}$, and the photocurrent density at $1.23 V_{\text{RHE}}$ was increased to $\sim 2.78 \text{ mA cm}^{-2}$ (ESI Fig. S20†). To measure the PEC performance of the scaled-up $\text{OEC}_{\text{Dip-TA}}/\text{BiVO}_4$ photoanode, back illumination was selected to reduce the diffusion path of H^+ and OH^- ions in the electrolyte (ESI Fig. S21†). As shown in Fig. 4b (see details in ESI Fig. S22†), similar to the small-scale BiVO_4 photoanode, the presence of uniformly coated OEC layer notably improved the PEC performance of the scaled-up photoanode. The scaled-up photoanode achieved a photocurrent density of $\sim 2.23 \text{ mA cm}^{-2}$ at $1.23 V_{\text{RHE}}$ and $\sim 0.83\%$ solar-to-hydrogen (STH) conversion efficiency at $0.65 V_{\text{RHE}}$.

It's worth noting that, under back illumination, diffusion of generated oxygen was difficult and accumulated gas bubbles would adsorb on the surface of the photoanode, leading to degradation in photocurrent density with the increase of covering factor (ESI Fig. S23†). Theoretical studies indicated that bubble formation and accumulation on the surface of

photoanodes are responsible for the poor stability of scaled-up photoanodes.^{20,21} Therefore, the stability test of the scaled-up BiVO_4 photoanode was conducted in a test system with water circulation, and the reactor was placed at $\sim 22^\circ$ to promote diffusion of generated oxygen (ESI Fig. S24†). As shown in Fig. 4c, the scaled-up $\text{OEC}_{\text{Dip-TA}}/\text{BiVO}_4$ photoanode showed $<4\%$ decay after operating under harsh conditions (at $\sim 0.6 V_{\text{RHE}}$ with continuous light illumination) for 5 h. After the stability test, a small-scale photoanode was taken from the scaled-up $\text{OEC}_{\text{Dip-TA}}/\text{BiVO}_4$ photoanode. Measured with a monochromator (see details in the ESI†), the result showed that it achieved a $\sim 90\%$ incident photon-to-electron conversion efficiency (IPCE) at 360 nm and $1.23 V_{\text{RHE}}$ (Fig. 4d).

3. Conclusions

In summary, a simple, efficient and scalable preparation method was promising for preparing large-scale high-performance BiVO_4 photoanodes for practical solar water splitting. Firstly, the uniform scaled-up BiOI film was successfully prepared *via* a SCDDR-ED method with a tilt-electrode-configuration. Particularly, the spatial-current-density-distribution in the FTO substrate regulated by changing electrode configurations was studied both experimentally and computationally. Increasing the electrode angle between FTO WE and Pt CE was conducive to improve the homogeneity of distributed current density in the FTO substrate. After that, the as-prepared BiOI film was covered with a thin vanadium source layer before annealing and then converted to BiVO_4 film *via* a MTCC method, to ensure the successful conversion of the BiOI film to the BiVO_4 film without affecting the uniformity. Hereto, the uniform scaled-up BiVO_4 photoanode was prepared for the first time. Finally, PEC performances for sulfite oxidation and water oxidation of BiVO_4 and OEC/BiVO_4 photoanodes were recorded. The photocurrent density ($\sim 2.55 \text{ mA cm}^{-2}$ at $1.23 V_{\text{RHE}}$) for sulfite oxidation of the 54.32 cm^2 BiVO_4 photoanode was the highest value yet reported, and it was comparable with that of the 1.66 cm^2 BiVO_4 photoanode ($\sim 2.85 \text{ mA cm}^{-2}$ at $1.23 V_{\text{RHE}}$). The slight decrease confirmed the excellent uniformity of the scaled-up BiVO_4 photoanode, indicating good enough scalability and reproducibility of the preparation method. To reduce resistive losses and improve the homogeneity of distributed potential in the FTO substrate, metal grids were deposited on the BiVO_4 photoanode *via* thermal evaporation. As a result, the maximum fill factor of the photocurrent density curve of the scaled-up BiVO_4 photoanode was raised from ~ 29 to $\sim 44.5\%$. In order to find out an appropriate method to accomplish OEC loading on the BiVO_4 photoanode, a NiFe-based OEC was prepared by four different methods. Results indicated that the $\text{OEC}_{\text{Dip-TA}}/\text{BiVO}_4$ photoanode, where BiVO_4 was dipped in a solution containing TA and $\text{Ni}^{2+}/\text{Fe}^{3+}$ ions, exhibited optimal activity and stability. The scaled-up $\text{OEC}_{\text{Dip-TA}}/\text{BiVO}_4$ photoanode achieved a photocurrent density of $\sim 2.23 \text{ mA cm}^{-2}$ at $1.23 V_{\text{RHE}}$ and $\sim 0.83\%$ STH conversion efficiency at $0.65 V_{\text{RHE}}$ under back illumination. In the end, a test system with water circulation was designed to solve the bubble accumulation problem that occurred during the stability test under

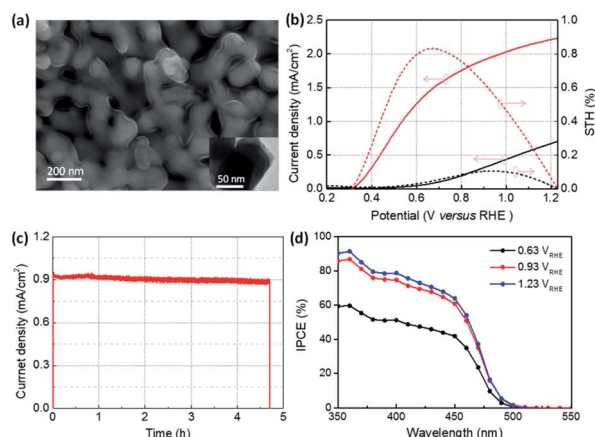


Fig. 4 (a) SEM image of the $\text{OEC}_{\text{Dip-TA}}/\text{BiVO}_4$ film. (b) PEC performances (water oxidation) of BiVO_4 (33.52 cm^2 , black) and $\text{OEC}_{\text{Dip-TA}}/\text{BiVO}_4$ (41.18 cm^2 , red) photoanodes: LSV scans for J_C , and STH conversion efficiency derived from J_C . (c) Stability test of the scaled-up $\text{OEC}_{\text{Dip-TA}}/\text{BiVO}_4$ photoanode at $\sim 0.6 V_{\text{RHE}}$ in borate buffer electrolyte. (d) IPCE spectra of a small-scale $\text{OEC}_{\text{Dip-TA}}/\text{BiVO}_4$ photoanode.

back illumination. The scaled-up OEC_{Dip-TA}/BiVO₄ photoanode showed <4% decay after operating under harsh conditions (at ~0.6 V_{RHE} with continuous light illumination) for 5 h.

In future research, to further improve PEC performances of scaled-up BiVO₄ photoanodes, various strategies, including introducing dopants and constructing composite structures, should be utilized to reduce charge carrier recombination caused by slow carrier separation and transport of BiVO₄.²⁷ Moreover, controllably scaling up high-performance photocathodes, which operated with scaled-up BiVO₄ photoanodes to meet the requirements of overall water splitting, was important to build integrated systems without external electronics. Finally, the fundamental cell with an electrode area of 9 × 10 cm² should be assembled to large scales for practical application, and other system components should also be considered, including structural support for cells, manifolds and pipes to conduct fluids, gas compression, storage tanks, water purification, and monitoring system.⁴

Conflicts of interest

There are no conflicts to declare.

Acknowledgements

This work was supported by the Basic Science Center Project of NSFC (51788104), and National Key Research and Development Program of China (2017YFB1104300).

References

- M. G. Walter, E. L. Warren, J. R. McKone, S. W. Boettcher, Q. Mi, E. A. Santori and N. S. Lewis, *Chem. Rev.*, 2010, **110**, 6446–6473.
- T. Hisatomi, J. Kubota and K. Domen, *Chem. Soc. Rev.*, 2014, **43**, 7520–7535.
- B. A. Pinaud, J. D. Benck, L. C. Seitz, A. J. Forman, Z. Chen, T. G. Deutsch, B. D. James, K. N. Baum, G. N. Baum, S. Ardo, H. Wang, E. Millere and T. F. Jaramillo, *Energy Environ. Sci.*, 2013, **6**, 1983–2002.
- R. Sathre, C. D. Scown, I. W. R. Morrow, J. C. Stevens, I. D. Sharp, I. J. W. Ager, K. Walczak, F. A. Houleae and J. B. Greenblatt, *Energy Environ. Sci.*, 2014, **7**, 3264–3278.
- M. Schröder, K. Kailasam, J. Borgmeyer, M. Neumann, A. Thomas, R. Schomäcker and M. Schwarze, *Energy Technol.*, 2015, **3**, 1014–1017.
- Y. Goto, T. Hisatomi, Q. Wang, T. Higashi, K. Ishikiriya, T. Maeda, Y. Sakata, S. Okunaka, H. Tokudome, M. Katayama, S. Akiyama, H. Nishiyama, Y. Inoue, T. Takewaki, T. Setoyama, T. Minegishi, T. Takata, T. Yamada and K. Domen, *Joule*, 2018, **2**, 509–520.
- J.-P. Becker, B. Turan, V. Smirnov, K. Welter, F. Urbain, J. Wolff, S. Haas and F. Finger, *J. Mater. Chem. A*, 2017, **5**, 4818–4826.
- B. Turan, J.-P. Becker, F. I. Urbain, F. Finger, U. Rau and S. Haas, *Nat. Commun.*, 2016, **7**, 12681.
- X. Yao, D. Wang, X. Zhao, S. Ma, P. S. Bassi, G. Yang, W. Chen, Z. Chen and T. Sritharan, *Energy Technol.*, 2018, **6**, 100–109.
- H. Lu, V. Andrei, K. J. Jenkinson, A. Regoutz, N. Li, C. E. Creissen, A. E. H. Wheatley, H. Hao, E. Reisner, D. S. Wright and S. D. Pike, *Adv. Mater.*, 2018, **30**, 1804033.
- S. H. Kristine Rodulfo Tolod and N. Russo, *Catalysts*, 2017, **7**, 13.
- C. W. Kim, Y. S. Son, M. J. Kang, D. Y. Kim and Y. S. Kang, *Adv. Energy Mater.*, 2016, **6**, 1501754.
- T. W. Kim and K.-S. Choi, *Science*, 2014, **343**, 990–994.
- T. W. Kim, Y. Ping, G. A. Galli and K.-S. Choi, *Nat. Commun.*, 2015, **6**, 8769.
- M. Huang, C. Li, L. Zhang, Q. Chen, Z. Zhen, Z. Li and H. Zhu, *Adv. Energy Mater.*, 2018, **8**, 1802198.
- V. Andrei, R. L. Z. Hoyer, M. Crespo-Quesada, M. Bajada, S. Ahmad, M. D. Volder, R. Friend and E. Reisner, *Adv. Energy Mater.*, 2018, **8**, 1801403.
- S. Hernández, G. Gerardi, K. Bejtka, A. Fina and N. Russo, *Appl. Catal., B*, 2016, **190**, 66–74.
- A. Hankin, F. E. Bedoya-Lora, C. K. Ong, J. C. Alexander, F. Petter and G. H. Kelsall, *Energy Environ. Sci.*, 2017, **10**, 346–360.
- C. Carver, Z. Ulissi, C. K. Ong, S. Dennison, G. H. Kelsall and K. Hellgardt, *Int. J. Hydrogen Energy*, 2012, **37**, 2911–2923.
- S. Hernández, G. Barbero, G. Saracco and A. L. Alexe-Ionescu, *J. Phys. Chem. C*, 2015, **119**, 9916–9925.
- A. S. Gliozzi, S. Hernández, A. L. Alexe-Ionescu, G. Saracco and G. Barbero, *Electrochim. Acta*, 2015, **178**, 280–286.
- A. A. Ojo and I. M. Dharmadasa, *Coatings*, 2018, **8**, 262.
- K. J. McDonald and K.-S. Choi, *Energy Environ. Sci.*, 2012, **5**, 8553–8557.
- Y. Kuang, Q. Jia, H. Nishiyama, T. Yamada, A. Kudo and K. Domen, *Adv. Energy Mater.*, 2016, **6**, 1501645.
- R. Sarala, M. A. Islam, S. B. Rabin and D. M. Stanbury, *Inorg. Chem.*, 1990, **29**, 1133–1142.
- X. Yao, X. Zhao, X. Li, D. Wang, A. I. Y. Tok, Z. Chen and T. Sritharan, *Joule*, 2019, **3**, 305–310.
- F. F. Abdi, T. J. Savenije, M. M. May, B. Dam and R. van de Krol, *J. Phys. Chem. Lett.*, 2013, **4**, 2752–2757.